SCIENCE CHINA
Technological Sciences

July 2013 Vol.56 No.7: 1629–1635
doi: 10.1007/s11431-013-5244-z

Characteristics of entropy generation and heat transfer in a microchannel with fan-shaped reentrant cavities and internal ribs

XIA GuoDong*, ZHAI YuLing & CUI ZhenZhen

Key Laboratory of Enhanced Heat Transfer and Energy Conservation, Ministry of Education, College of Environmental and Energy Engineering, Beijing University of Technology, Beijing 100124, China

Received December 28, 2012; accepted April 18, 2013; published online May 24, 2013

Three-dimensional laminar fluid flow and heat transfer in a micro heat sink with cavities and internal ribs are investigated using numerical methods. Moreover, according to the second law of thermodynamics, the model of entropy generation is also established for variable cross section of the microchannel. The simulation encompasses Reynolds number of 198–600, relative cavity height e_1/D_h values of 0–0.65, relative rib height e_2/D_h range of 0–0.2167. The results show that the effect of relative rib height on entropy generation is significant, while the relative cavity height has little effect on it. The combined effect of cavities and ribs in the microchannel has better performance of heat transfer than the smooth microchannel under similar conditions. Extensive simulations are conducted to collect data on the characteristics of heat transfer and fluid flow in a micro heat sink with cavities and internal ribs. Using these data, correlations for Nusselt number and friction factor in terms of Reynolds number and the geometry of cavity and rib have been developed.

microchannel, entropy generation, heat transfer enhancement, variable cross section

Citation: Xia G D, Zhai Y L, Cui Z Z. Characteristics of entropy generation and heat transfer in a microchannel with fan-shaped reentrant cavities and internal ribs. Sci China Tech Sci, 2013, 56: 1629–1635, doi: 10.1007/s11431-013-5244-z

1 Introduction

With the development of the science and technology, the electronic device designs chase for the performance of the lower power consumption, higher stability and reliability, as well as higher integration and super-miniaturization. However, the cooling of the device has also become a major challenge [1]. The micro heat sink was first presented by Tuckerman in 1981 [2], and it can remove heat efficiently because of the high surface to volume ratio, and the cooling effect is obvious. It has been widely used in the areas of electronic chip cooling, aerospace, bio-engineering, material science, and high-temperature superconductors and so on. According to the need for additional input power, it can be divided into active method and passive method to enhance heat transfer in the microchannel. However, the passive method has been given more attention by many authors because it can enhance heat transfer only by changing the shape of channel, adding ribs and placing turbulator inside channel, etc. [3–5].

Many studies have focused on the relationship between thermal resistance and pressure drop in the past decades. Bejan first presented the optimization of heat sink using entropy generation minimization. The method was based on the second law of thermodynamics, which was accepted by more and more authors [6]. Haddad et al. [7] numerically investigated steady laminar forced convection fluid flow through the parallel plates microchannel. They analyzed the effect of *Kn* number, *Re* number and *Pr* number on heat transfer and entropy generation. Ko [8] numerically analyzed laminar forced convective flow and entropy genera-

*Corresponding author (email: xgd@bjut.edu.cn)

tion in a 180° curved rectangular duct with longitudinal ribs. The results showed that the existence of rib can reduce the entropy generation from heat transfer irreversibility since the secondary vortices are augmented by the rib and temperature gradient is smoother, so the heat transfer performance is enhanced. Xia et al. [9] investigated the fluid flow through the microchannel with periodically changeable cross sections using CFD. Moreover, they analyzed the influence of structural parameters on depth. The results revealed that heat transfer enhancement can be attributed to the flow disturbance near wall, adverse pressure gradient in the reentrant cavities, the jet and throttling effects. Wang et al. [10] investigated the effect of *Nu* number, *f* number, heat enhancement factor η and augmentation entropy generation number $N_{s,a}$ on the heat transfer and entropy generation. The results indicated that the internal longitudinal fins enhanced the secondary flows and increased the temperature gradient near the wall, which in turn increased the heat transfer. Eiamsa-ard et al. [11] experimentally examined the effect of the rib-grooved channel on turbulently forced convection heat transfer. They presented three types of rib-groove arrangements: rectangular rib-triangular groove, triangular rib-rectangular groove, triangular rib-triangular groove. The results showed that heat transfer performance of the combined microchannel was better than that of the smooth channel and the effect of different pitch ratio on flow and heat transfer was also studied. Hans et al. [12] experimentally studied the characteristics of flow and heat transfer on the absorber plate with multiple V-type roughness. They examined the effect of Reynolds number, relative roughness height, relative roughness pitch and relative roughness width and angle of attack on heat transfer. Then the correlations of Nusslet number and friction factor were developed by using experimental data. Generally speaking, the rib-groove in the microchannel can be seen as turbulator, which can disturb the viscous sub-layer and reduce the thickness of boundary layer [13].

Based on the above analysis, the main purpose of this paper is to numerically investigate the combined effect of reentrant cavity and rib on fluid flow and heat transfer in the microchannel. Based on the second law of thermodynamics, the model of entropy generation is established and the effect of Reynolds number, relative reentrant cavity height and relative rib height on flow is also analyzed. Then, the correlations of *Nu* number and *f* number are presented according to the numerical data.

2 Model of entropy generation

2.1 Description of model

The geometry of the microchannel heat sink with reentrant cavities and internal ribs is shown in Figure 1(a). The microchannel is composed of fan-shpaed reentrant cavity and rib in the sidewall, which contains 10 parallel silicon-based microchannels. The length L, width W, and height of bottom h and channel H are 10, 3, 0, 15 and 0.2 mm, respectively. A constant heat flux is applied at the bottom wall (q_w=10^6 W m^{-2}), while other walls are adiabatic. The cross section of single channel is shown in Figure 1(b), and water is used as working fluid. The width of single chanel W_{ch}, wall channel pitch W_b and hydraulic diameter D_h are 0.1, 0.2 and 0.133 mm, respectively. The curvatures of circular arc, θ_1 and θ_2, are varied from 50° to 180° and 40° to 110°, respectively. The length of L_1, L_2 and L_3 are 0.1732, 0.1 and 0.4 mm, respectively. Therefore, the relative reentrant cavity height e_1/D_h and relative rib height e_2/D_h are varied from 0 to 0.65 and 0 to 0.2167, respectively.

2.2 Establishing the model of entropy generation

The cross section of the microchannel is continuously changed along the longitudinal direction in the microchannel. Considering an arbitrary control volume in the microchannel, the model of entropy generation rate is established based on the second law of thermodynamics, as shown in Figure 2.

Considering an arbitrary control volume (CV) in the microchannel, the entropy generation rate caused by heating bottom can be divided into two processes: 1) entropy generation rate caused by the heat exchange between fluid and the bottom of heat sink; 2) entropy generation rate due to friction loss when fluid flows through adiabatic duct. According to the law of second thermodynamics, the entropy generation rate of process 1) due to the heat transfer between cool and hot walls can be calculated by the following equations [14]:

$$\dot{S}_{\Delta T} = \frac{\dot{Q}}{T_f} - \frac{\dot{Q}}{T_b} = \frac{\dot{Q}(T_b - T_f)}{T_f T_b}, \tag{1}$$

$$\dot{Q} = q_w A_{film}, \tag{2}$$

where T_b, T_f are the average temperature of the bottom of the heat sink and fluid, respectively, K; $\dot{Q}$ is the total heat transfer of the bottom of heat sink, W; A_{film} is the heating area of heat sink, m^2.

The entropy generation rate of process 2) caused by adiabatic flow can be divided into: (a) entropy generation rate caused by the irreversibility; (b) entropy generation rate caused by mass flow through control volume. Therefore, according to the first and second laws of thermodynamics, the entropy generation rate due to fluid flow through adiabatic duct can be expressed as follows:

$$\frac{dQ_{CV}}{dt} = \dot{m}\left(dh + \frac{1}{2}du^2 + g dz\right), \tag{3}$$

$$\frac{dS}{dt} = \dot{m} ds + d\dot{S}_{\Delta p}, \tag{4}$$

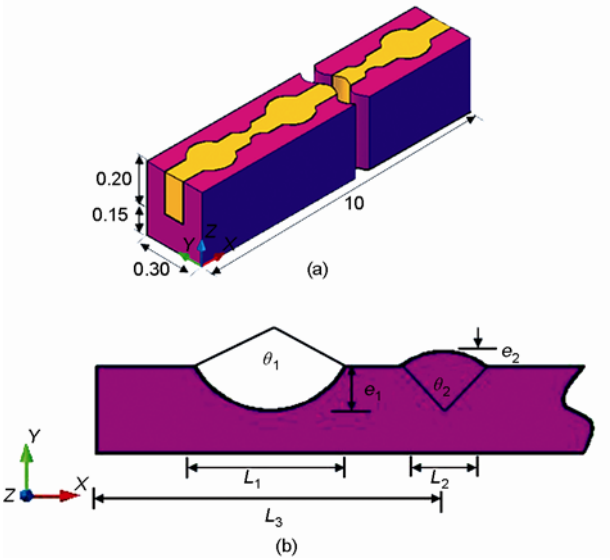

Figure 1 Three-dimensional single microchannel (a) and cross section (b). (unit: mm)

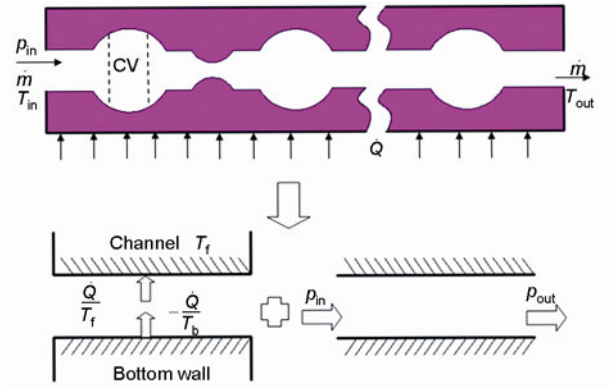

Figure 2 Model of entropy generation of the microchanel with variable cross section.

where Q_{CV} is the energy of system, kJ; s and h are the specific enthalpy and specific entropy, respectively, kJ (kg K)$^{-1}$, kJ kg^{-1}; $\dot{m}$ is the mass flow, kg s^{-1}; since the flow is steady and incompressible, the change of kinetic and potential energies is negligible, i.e., $\frac{dQ_{CV}}{dt}=0$ and $\frac{dS}{dt}=0$. Hence, eqs. (3) and (4) can be reduced to

$$dh = 0, \tag{5}$$

$$d\dot{S}_{\Delta p} = -\dot{m}ds. \tag{6}$$

In addition,

$$dh = T_f ds + \frac{1}{\rho}dp. \tag{7}$$

By combining eqs. (5)–(7), the entropy generation rate caused by flow can be expressed with the following formula:

$$\dot{S}_{\Delta P} = -\dot{m}\left(\int_{p_{in}}^{P_{out}} \frac{1}{\rho T_f} dP\right) = \frac{\dot{m}}{\rho T_f}\Delta P. \tag{8}$$

Further, by combining eqs. (1)–(8), the total entropy generation rate due to the fluid flow through heating bottom of heat sink can be arranged to give

$$\dot{S}_{gen} = \dot{S}_{\Delta T} + \dot{S}_{\Delta p} = \frac{\dot{Q}(T_b - T_f)}{T_f T_b} + \frac{\dot{m}}{\rho T_f}\Delta p, \tag{9}$$

where Δp, ρ and V are the pressure drop between inlet and outlet, density and volume, Pa, kg m^{-3}, m^3, respectively.

To quantize the entropy generation rate, we define the augmentation entropy generation number,

$$N_{s,a} = \dot{S}_{gen} / \dot{S}_{gen,0}, \tag{10}$$

where $\dot{S}_{gen,0}$ is the total entropy generation rate of the reference microchannel. Here, the smooth rectangular microchannel with the same dimension is considered as reference microchannel. Augmentation techniques yielding values of $N_{s,a}$ less than unity are thermodynamically advantageous since in addition to enhancing heat transfer they reduce the irreversibility of the microchannel.

3 Simulation approach

3.1 Mathematical model and method

The temperature and pressure drop contained in eq. (9) can be solved by the continuity, momentum and energy equations. Three-dimensional conjugate heat transfer between silicon-based channel wall and liquid is computed over the entire microchannel. Following are some of the assumptions made in the simulation: 1) negligible axial heat conduction and natural convection; 2) constant solid and fluid properties except the water viscosity.

For fluid zone, the vector forms of continuity equation, momentum equation and energy equation are written as

$$\nabla \boldsymbol{V} = 0, \tag{11}$$

$$\rho(\boldsymbol{V}\nabla\boldsymbol{V}) = -\nabla p + \nabla(\mu\nabla\boldsymbol{V}), \tag{12}$$

$$\rho c_p(\boldsymbol{V}\nabla T) = \lambda_f \nabla^2 T. \tag{13}$$

For solid zone,

$$\nabla \boldsymbol{V} = 0, \tag{14}$$

$$\lambda_s \nabla^2 T = 0, \tag{15}$$

where μ, c_p, λ_f and λ_s are the fluid of dynamic viscosity, specific heat, conductivity and the solid of conductivity, respectively, kg (m s)$^{-1}$, kJ (kg K)$^{-1}$, W (m K)$^{-1}$ and W (m K)$^{-1}$.

A constant and uniform velocity and temperature (T_{in}= 293 K) are applied at the inlet of microchannel. The velocity varies from 1 to 4 m s^{-1} and the corresponding Reynolds number varies from 198 to 600. At the outlet, the static pressure is zero. The boundary conditions used are symmetric at two side planes. Based on the above equations, the solution is regarded as convergent when [15]

$$\mathrm{Max}\left|(\varphi^{i+1}-\varphi^{i})/\varphi^{i+1}\right| \leqslant 10^{-6}, \tag{16}$$

where φ represents variable, namely u, v, w or T, and i is the iteration number.

The equations mentioned above are all solved by a commercial computational fluid dynamic software CFD (FLUENT.6.3.26). A preprocessor GAMBIT is used to generate the meshes for the solver. The governing equations are discretized by using the finite control volume. The SIMPLEC algorithm is utilized to deal with the coupling of pressure and velocity.

3.2 Grid independence

In order to ensure the accuracy of numerical results, a test of grid independence must be examined before numerical computation. The computational domain is resolved by the nonregular elements. The characteristics of three grids: 338000, 625000 and 868000 cells, are used in the simulations to investigate the grid convergence index.

The axial velocity distribution in the centerline along the longitudinal direction and temperature distribution in the solid-liquid interface is shown in Figure 3. A maximum difference of less than 0.71% for axial velocity and 0.16% for temperature in the computed results between 625000 cells and 868000 cells is observed. Hence, 625000 cells are selected to conduct the calculation.

4 Results and discussion

4.1 Validation of model

In order to validate the numerical method, numerical simulation is carried out to predict the results obtained by theoretical study of Shan et al. [16] with the smooth rectangular microchannel. The equation of friction factor f on laminar convective heat transfer is written as

$$fRe = 96(1-1.3553\alpha_c+1.9467\alpha_c^2 -1.7012\alpha_c^3+0.9564\alpha_c^4-0.2537\alpha_c^5). \tag{17}$$

The equations of friction factor obtained from pressure drop [17] and temperature difference between the inlet and outlet obtained from energy balance are expressed as

$$f=\frac{2\Delta p D_h}{\rho L u_m^2}, \tag{18}$$

$$T_{out}-T_{in}=\frac{\dot{Q}}{\rho A u_m c_p}, \tag{19}$$

where α_c is the width to height ratio of the microchannel; u_m and c_p are the average velocity and specific heat of fluid, respectively, m s^{-1}, J $(kg\,K)^{-1}$; A is the inlet cross section of the microchannel, m^2.

The comparison of friction factor and temperature difference between the smooth rectangular microchannel and the microchannel with fan-shaped reentrant cavities and internal ribs (e_1/D_h=0.65 and e_2/D_h=0.2167) is shown in Figure 4. It is observed that the average difference is ±5% for friction factor and ±2.5% for temperature difference between numerical results and theoretical results, respectively. It can be seen that there is a very good agreement between present numerical model and theory. From the above validation test, we conclude that the present numerical code can correctly predict the basic characteristic of fluid flow through the microchannel with variable cross section. Figure 4 also shows that all the conditions are laminar depending on its Reynolds number range.

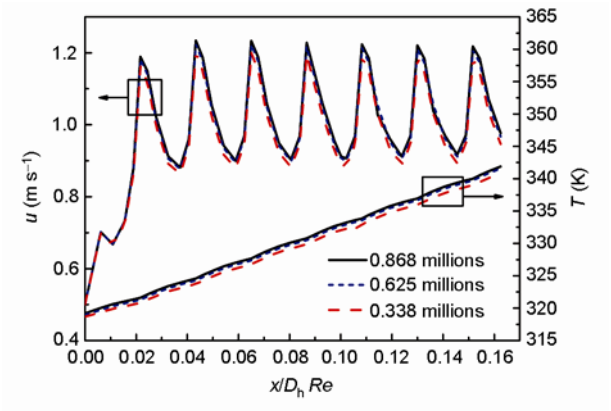

Figure 3 Validation of axial velocity distribution at centerline of microchannel and temperature distribution in the solid-fluid interface.

4.2 Analysis of entropy generation

Figures 5 and 6 exemplify the effect of Reynolds number on augmentation entropy generation number $N_{s,a}$ with different

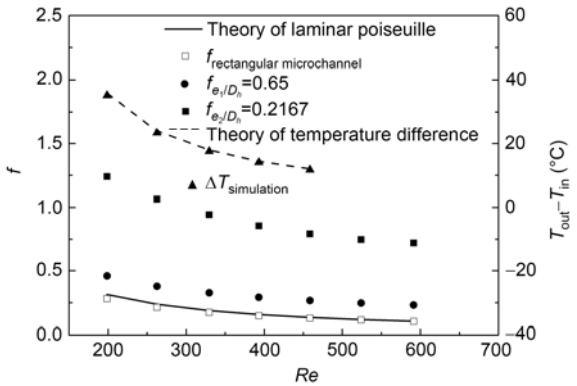

Figure 4 The validation of model.

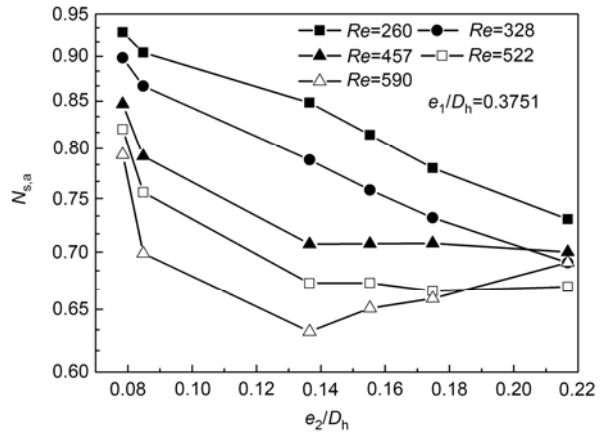

Figure 5 Effect of the relative rib height on augmentation entropy generation number.

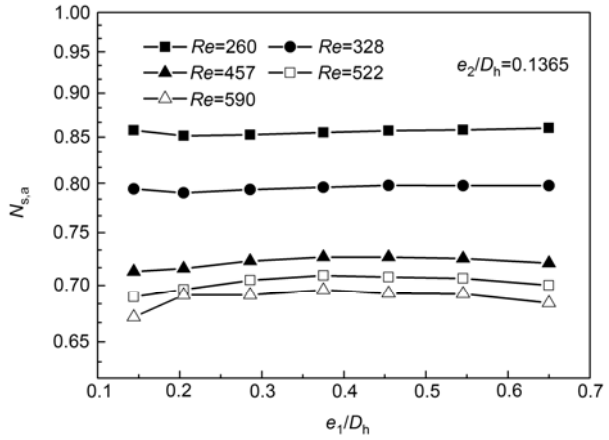

Figure 6 Effect of relative cavity height on augmentation entropy generation.

relative rib height and relative cavity height. It is clear that in comparison with the smooth rectangular microchannel, the microchannel with fan-shaped cavities and internal ribs can reduce entropy generation caused by flow. Although the pressure drop increases with the rise of Reynolds number for all the rib height, the effect of irreversibility caused by flow on total entropy generation is small due to the low velocity and small cross section in the microchannel. Since the dead time of fluid is longer in the reentrant cavity and hot and cold fluids cannot be fully mixed, the rise of temperature under low Reynolds number is lower than that under high Reynolds number in the center of microchannel. Therefore, the entropy generation of low Reynolds number is higher than that of high Reynolds number.

Moreover, from Figure 5 it is obvious that with increasing the relative rib height, $N_{s,a}$ first decreases dramatically when $e_2/D_h<0.09$, then decreases slowly. A maximum value of $N_{s,a}$ attains at $Re>328$, $e_2/D_h=0.1365$, then $N_{s,a}$ increases with the rise of the relative rib height. However, there is no minimum of entropy generation when $Re<328$. From Figure 6, $N_{s,a}$ has no change with the rise of e_1/D_h, depending on its range of Reynolds number. This phenomenon can be explained as: the area of stagnation zone increases with the rise of relative reentrant cavity height, however, the fluid has always been in the state of stagnation within the reentrant cavity and the effect on temperature in the center microchannel is not obvious.

4.3 Characteristic of flow and heat transfer

Figures 7 and 8 illustrate the effect of the Reynolds number on Nu/Nu_0 with different relative rib heights and relative reentrant cavity heights. Subscript 0 represents the smooth rectangular microchannel. The correlation of Nu number is defined as

$$h_{ave} = \frac{\dot{Q}}{NA_{ch}\Delta T}, \tag{20}$$

$$Nu = \frac{h_{ave}D_h}{\lambda_f}, \tag{21}$$

where h_{ave} is the average heat transfer coefficient, W $(m^2 K)^{-1}$; N is the number of the microchannel; A_{ch} is the contact area between the single microchannel and fluid, $A_{ch}=(W_{ch}+2H)L$, m^2; ΔT is the average temperature difference between bottom wall and fluid, $\Delta T=T_b-1/2(T_{in}+T_{out})$. T_{in} and T_{out} are the temperature of inlet and outlet, respectively, K.

Figure 7 shows the effect of relative rib height e_2/D_h on Nu number when $e_1/D_h=0.375$. It is obvious that all the values of Nu/Nu_0 are more than unity, so the heat transfer of the microchannel with reentrant cavities and internal ribs has better performance than the smooth microchannel. This is due to the increase of the contact area of hot and cold fluid with the existence of reentrant cavity. When water enters the cavity, the velocity decreases and the full heat exchange appears between cold fluid and wall channel. It can weaken the heat transfer [18] when dead time is longer in the reentrant cavity and the temperature of cold fluid is

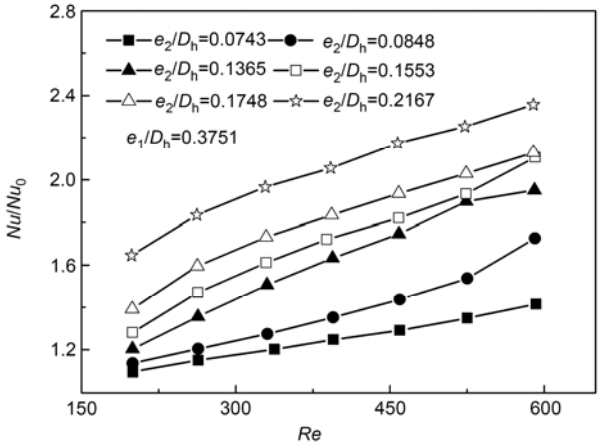

Figure 7 Effect of the relative rib height on Nu number.

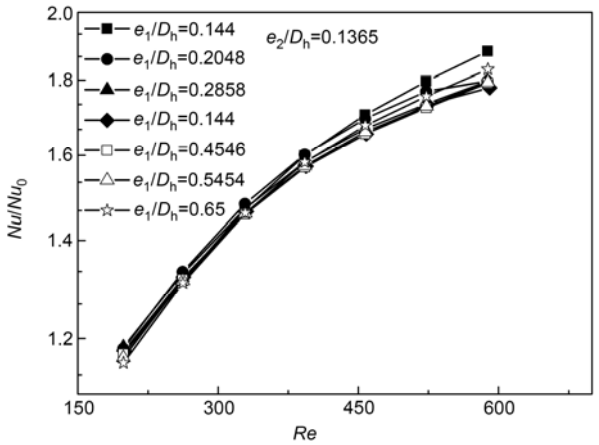

Figure 8 Effect of the relative cavity height on *Nu* number.

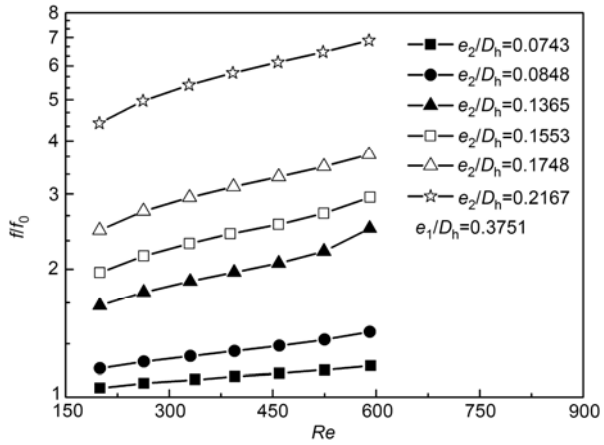

Figure 9 Effect of the relative rib height on *f* number.

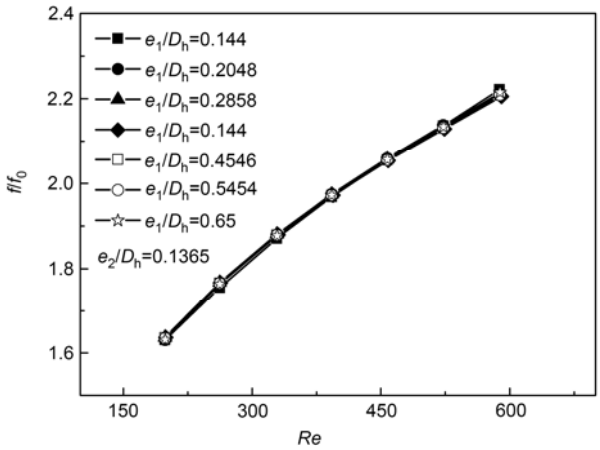

Figure 10 Effect of the relative cavity height on *f* number.

gradually increased under lower Reynolds number. However, adding ribs between the cavities can reduce cross section dramatically, which causes more energy to flow through the cavity under low Reynolds number. Moreover, the hydrodynamic and thermal layers are disturbed by the cavity and rib, so the heat transfer enhancement is more obvious.

Figure 8 shows the effect of the relative cavity height e_1/D_h on *Nu* when e_2/D_h=0.1365. From Figure 7, all the values of Nu/Nu_0 are more than unity. However, there is no change of Nu/Nu_0 with the rise of Reynolds number and the relative cavity height. Therefore, the effect of reentrant cavity on heat transfer is not obvious.

Figure 9 shows the effect of the relative rib height on friction coefficient when e_1/D_h=0.375. From Figures 9 and 10 it is obvious that the effect of rib on friction coefficient is relatively obvious. The friction coefficient increases by 3.6 times when the relative rib height is 2.9 times lager. However, the effect of the relative rib height on friction coefficient is not obvious.

As discussed before, the effect of the relative rib height and relative cavity height on *Nu* number and *f* number is obvious. Based on the numerical results, the correlations of *Nu* number and *f* number are developed:

$$Nu = 0.495Re^{0.6371}\left(\frac{e_1}{D_h}\right)^{-0.0008}\left(\frac{e_2}{D_h}\right)^{0.4166}, \quad 0 < e_1/D_h \leqslant 0.65, \quad 0 < e_1/D_h \leqslant 0.2167, \tag{22}$$

$$f = 90.0033Re^{-0.6629}\left(\frac{e_1}{D_h}\right)^{-0.0006}\left(\frac{e_2}{D_h}\right)^{0.8854}, \quad 0 < e_1/D_h \leqslant 0.65, \quad 0 < e_1/D_h \leqslant 0.0848, \tag{23}$$

$$f = 855.0918Re^{-0.6}\left(\frac{e_1}{D_h}\right)^{-0.0023}\left(\frac{e_2}{D_h}\right)^{2.2078}, \quad 0 < e_1/D_h \leqslant 0.65, \quad 0.0848 < e_1/D_h \leqslant 0.2167. \tag{24}$$

As shown in Figure 9, the variation of friction coefficient is greater when e_2/D_h>0.0848 than that when e_2/D_h<0.0848, so the friction coefficient can be divided into two parts. A comparison between the *Nu* number and *f* number obtained from numerical results and those predicted by the correlations have been shown in Figures 11 and 12, which shows that most of the predicted data points lie within ±10% deviation lines of the numerical results. Therefore, the correlations developed can predict the values of *Nu* number and friction factor with reasonable accuracy in the range of parameters investigated.

5 Conclusions

In this paper, according to the second law of thermodynamics, the model of entropy generation rate of a microchannel with fan-shaped reentrant cavities and internal ribs is established. Moreover, the effect of different structural parameters on laminar flow and heat transfer is investigated using numerical simulation. Based on the results presented above,

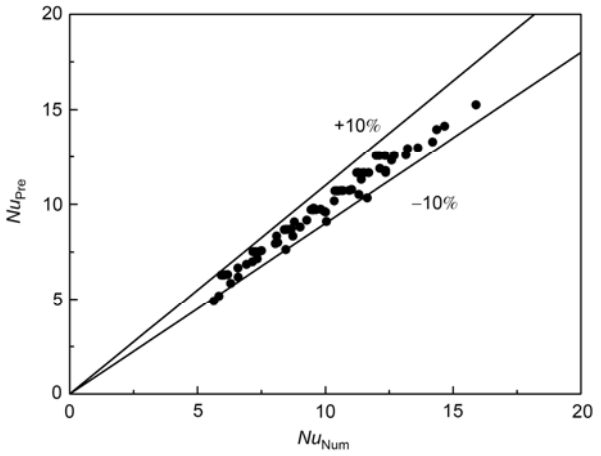

Figure 11 Comparison of numerical and theoretical *Nu* numbers.

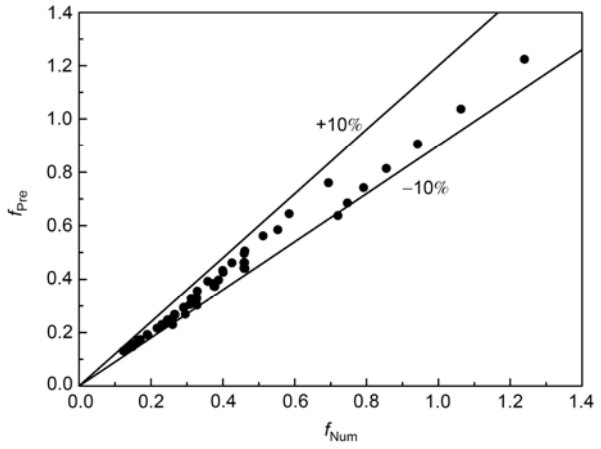

Figure 12 Comparison of numerical and predicted values of friction factor.

some essential conclusions are drawn below.

1) The model of entropy generation rate in a microchannel is established, and the effect of the relative rib height and relative cavity height on entropy generation is analyzed. The effect of relative rib height on entropy generation is more obvious than that of the relative cavity height depending on its range of Reynolds number.

2) The combined effect of cavity and rib can enhance heat transfer in the microchannel with fan-shaped reentrant cavities and internal ribs. Hence, the cold and hot fluids can be fully mixed in the reentrant cavity and can take hot fluid quickly. Moreover, due to the periodical cavities and ribs, the hydrodynamic and thermal layers are disturbed and the flow develops continuously.

3) The correlations of *Nu* number and *f* number in the microchannel with reentrant cavities and internal ribs are presented. These correlations have been found to predict the values with ±10% deviation.

1 Feng H J, Chen L G, Xie Z H, et al. Thermal insulation constructal optimization for steel rolling reheating furnace wall based on entransy dissipation extremum principle. Sci China Tech Sci, 2012, 55: 3322–3333

2 Tuckerman D B, Pease R F W. High-performance heat sinking for VLSI. IEEE Electron Device Lett, 1981, 2(5): 126–129

3 Bilen K, Cetin M, Gul H, et al. The investigation of groove geometry effect on heat transfer for internally grooved tubes. Appl Therm Eng, 2009, 29(4): 753–761

4 Mesalhy O M, Abdel Aziz S S, El-Sayed M M. Flow and heat transfer over shallow cavities. Int J Thermal Sci, 2010, 49(3): 514–521

5 Chai L, Xia G D, Zhou M Z, et al. Numerical simulation of fluid flow and heat transfer in a microchannel heat sink with offset fan-shaped reentrant cavities in sidewall. Int Commun Heat Mass Transfer, 2011, 38(5): 577–584

6 Bejan A, Tsatsaronis M, Moran M. Thermal Design and Optimization. New York: Wiley-Interscience Publication, 1996. 463–506

7 Haddad O, Abuzaid M, Al-Nimr M. Entropy generation due to laminar incompressible forced convection flow through parallel-plates microchannel. Entropy, 2004, 6(5): 413–426

8 Ko T H. Numerical investigation on laminar forced convection and entropy generation in a curved rectangular duct with longitudinal ribs mounted on heated wall. Int J Thermal Sci, 2006, 45(4): 390–404

9 Xia G D, Chai L, Yang R B, et al. Influence of structural parameters on fluid flow and heat transfer in microchannel with periodically changeable cross-sections (in Chinese). J Chem Indus Eng, 2009, 60(11): 2705–2711

10 Wang F, Wang G. Heat transfer augmentation and entropy generation analysis of a helically coiled tube with internal longitudinal fins. Chem Eng Technol, 2011, 34(11): 1876–1882

11 Eiamsa-ard S, Promvonge P. Thermal characteristics of turbulent rib-grooved channel flows. Int Commun Heat Mass Transfer, 2009, 36(7): 705–711

12 Hans V S, Saini R P, Saini J S. Heat transfer and friction factor correlations for a solar air heater duct roughened artificially with multiple V-ribs. Sol Energy, 2010, 84(6): 898–911

13 Jaurker A R, Saini J S, Gandhi B K. Heat transfer and friction characteristics of rectangular solar air heater duct using rib-grooved artificial roughness. Sol Energy, 2006, 80(8): 895–907

14 Bejan A. Entropy Generation Through Heat and Fluid Flow. New York: Wiley-Interscience Publication, 1982. 89–190

15 Qu W, Mudawar I. Experimental and numerical study of pressure drop and heat transfer in a single-phase micro-channel heat sink. Int J Heat Mass Transfer, 2002, 45(12): 2549–2565

16 Shah R K, London A L. Laminar Flow Forced Convection in Ducts, Supplement 1. New York: Academic Press, 1978. 17–36

17 Steinke M E, Kandlikar S G. Single-phase liquid friction factors in microchannels. Int J Thermal Sci, 2006, 45(11): 1073–1083

18 Chai L, Xia G D, Zhou M Z. Effects of structural parameters on fluid flow and heat transfer in a microchannel with aligned fan-shaped reentrant cavities. Int J Thermal Sci, 2011, 50(3): 411–419